System Design and Application of Magnetostrictive Biosensor

(磁致伸缩生物传感器系统设计和应用)

Zhang Kewei
Zhang Shaoqin

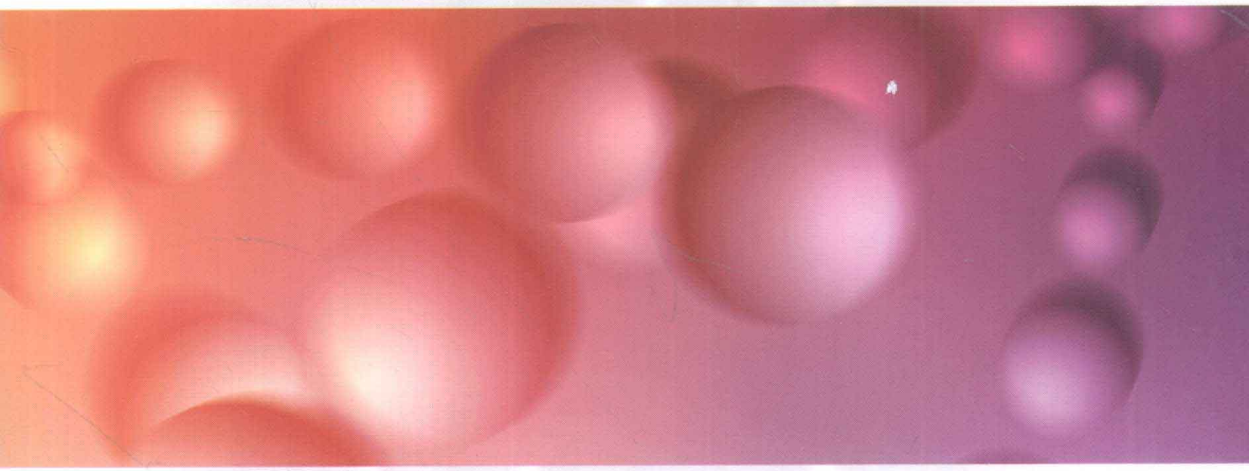

SCIENCE PRESS
Beijing

System Design and Application of Magnetostrictive Biosensor

(磁致伸缩生物传感器系统设计和应用)

Zhang Kewei
Zhang Shaoqin

科学出版社
Science Press

Responsible Editors: Qian Jun, Liu Xinli

16 Donghuangchenggen North Str.
Beijing, China

Published by Science Press Ltd.

ISBN: 978-7-03-032532-7

Preface

Food-borne disease caused by pathogenic bacteria is a major concern all over the world, and it attracts a great of attention of people and the governments, relevant international organizations and academic institutions. Therefore, there is an urgent need for detection technologies that can rapidly detect/monitor the presence of pathogens in food. Various detection technologies have been recently developed and investigated. Among these technologies, biosensor technologies provide many unique advantages over others.

In this book, the knowledge about magnetostrictive biosensor system design and applications of magnetostrictive biosensors for bacterial detection were introduced.

Chapter 1 introduced the background of food safety and security, the basic knowledge about pathogenic bacteria and food-borne illness and also the knowledge about conventional bacterial detection methods and advanced biosensor techniques. Regarding biosensors, electrochemical biosensors, acoustic wave (AW) biosensors and micro-cantilever (MC) based biosensors were discussed. In addition, recently developed magnetostrictive micro-cantilever (MSMC)-based biosensors and magnetostrictive particle (MSP) based biosensors were also introduced.

Chapter 2 introduced the resonance behavior and influence of surrounding media on the resonance behavior of MSP based sensors. The resonance behavior of MSP sensors in viscous media is unveiled. In this chapter, both resonance frequency and Q value of MSP based sensors in different sizes/dimensions and in different media were investigated.

Chapter 3 introduced the techniques in design and fabrication of phage/antibody immobilized magnetostrictive biosensor for bacterial detection. Using an MSP as a sensor platform, an MSP based biosensor has many unique advantages, such as wireless, high sensitivity, easy operation, and working well in liquid. In this chapter, phage immobilized MSP biosensors for the detection of *S. typhimurium* and antibody-immobilized MSP biosensors for the detection of *E. coli* and *L. Monocytogenes* are fully presented.

Chapter 4 introduced the design and simulating technique for advanced portable MSP biosensor system. Two different techniques are introduced: one is based on

frequency-domain technique, and the other one is based on time-domain technique. A special simulating technique based on the equivalent circuit using MATLAB to analyse the resonance behavior (i.e. phase and gain) is introduced. The application of the two techniques for bacterial detection was also presented in this chapter.

One of the final goals of MSP based biosensors is to be able to detect a target with extremely small mass such as virus. In this case, the sensor size has to be decreased down to nano-scale. However, it is difficult to decrease the size of currently commercial available magnetostirctive material down to nano-scale. In Chapter 5, a template based electro-chemical deposition method was introduced for the synthesis of amorphous magnetostrictive nanowires to obtain a highly sensitive biosensor platform.

Chapter 6 introduced the future perspectives of magnetostrictive biosensor system and also gave some suggestions to further improve the performance of magnetostrictive biosensor system.

The authors would like to express our appreciation to the Shanxi Province Government, Taiyuan University of Science and Technology, Auburn University and Professors Z. Y. Cheng, Bryan A. Chin and other colleges acknowledged in Dr. Kewei Zhang's doctoral dissertation.

List of Abbreviations

FDA	Food and drug administration
CDC	Centers for disease control and prevention
ELISA	Enzyme-linked immunosorbent assay
PCR	Polymerase chain reaction
DNA	Deoxyribonucleic acid
SPR	Surface plasmon resonance
ISE	Ion-selective electrode
ISFET	Ion-sensitive field effect transistors
AW	Acoustic wave
QCM	Quartz crystal microbalance
TSM	Thickness shear microbalance
SAW	Surface acoustic wave
IDT	Interdigital transducer
APM	Acoustic wave plate mode
SH-APM	Shear-horizontal acoustic wave plate mode
FPW	Flexural plate wave
MC	Micro-cantilever
MSMC	Magnetostrictive micro-cantilever
AC	Alternating current
DC	Direct current
PAbs	Polycolonal antibodies
MAbs	Monoclonal antibodies
MSP	Magnetostrictive particles
NSB	Non-specific binding
BSA	Bovine serum albumin
PBS	Phosphate buffered saline
TBS	Tris buffered saline
PC	Personal computer
SEM	Scanning electron microscopy
EDTA	Ethylenediaminetetraacetic acid

DUT	Device under test
GUI	Graphical user interface
FCC	Face centered cubic

List of Symbols

S_m	Mass sensitivity
Q	Quality merit factor
f_n	n^{th} harmonic resonance frequency
L	Length
W	Width
v	Acoustic velocity
E	Young's modulus
ρ	Density
υ	Poisson ratio
m	Power value
$U^*(\omega)$	Potential through DUT
$U_r^*(\omega)$	Potential through a reference
$Z^*(\omega)$	Impedance of DUT
$Z_r^*(\omega)$	Impedance of a reference
F	Faraday
H	Henry
Ω	Ohm
f_r	Resonance frequency
f_{ar}	Anti-resonance frequency

Contents

Preface ..... **i**
List of figures ..... **vii**
List of tables ..... **xv**
List of abbreviations ..... **xvii**
List of symbols ..... **xix**
1 Introduction **1**
1.1 Introduction to pathogenic bacteria and food-borne illness 1
1.1.1 Foodborne pathogenic bacteria 1
1.1.2 Infectious dose and detection of bacteria 4
1.2 Conventional bacterial detection methods 5
1.2.1 Plate counting methods 5
1.2.2 Enzyme-linked immunosorbent assay (ELISA) 6
1.2.3 Polymerase chain reaction (PCR) 7
1.3 Biosensors 9
1.3.1 Optical biosensors 10
1.3.2 Electrochemical biosensors 12
1.3.3 Acoustic wave (AW) biosensors 14
1.3.4 Micro-cantilever (MC) based biosensors 19
1.3.5 Magnetostrictive micro-cantilever (MSMC)-based biosensors 22
1.4 Magnetostrictive particle (MSP) based biosensors 23
1.4.1 Resonance behavior of MSP 23
1.4.2 Resonance behavior of MSP in viscous media 25
1.4.3 Magnetostrictive effect and materials 26
1.4.4 Current status of biosensors based on MSPs 28
1.5 Sensing element for biosensors—antibodies vs. phages 28
1.6 Research objectives 30
References 31
2 Resonance behavior of msp and influence of surrounding media **37**
2.1 Introduction 37
2.2 Characterization of the resonance behavior of an MSP 37

2.3 Materials and methods 39
2.4 Results and discussion 40
2.4.1 Resonance frequency of MSPs 40
2.4.2 The Q value of MSPs 42
2.4.3 Resonance frequency of MSP in liquid 43
2.4.4 Determination of surface roughness R_{ave} 46
2.4.5 Factors that affect the measured surface roughness R_{ave} 48
2.4.6 Effect of liquid on Q value 52
2.5 Conclusions 54
References 55
3 Techniques in design and production of phage/antibody immobilized magnetostrictive biosensor for bacterial detection 56
3.1 Introduction 56
3.2 MSP preparation 57
3.3 Phage and antibody immobilization 57
3.3.1 Phage immobilization 57
3.3.2 Antibody immobilization 57
3.4 Blocking agents 59
3.5 Preparation of bacterial culture 59
3.6 Experimental setup 60
3.7 SEM observation 62
3.8 Hill plot and kinetics of binding 62
3.9 Results and discussion 65
3.9.1 Detection of *S. typhimurium* 65
3.9.2 Detection of *E. coli* 67
3.9.3 Detection of *S. aureus* 69
3.9.4 Detection of *L. Monocytogenes* 70
3.10 Conclusions 73
References 74
4 Design and simulating techniques for portable msp biosensor system 75
4.1 Introduction 75
4.2 Equivalent circuit of magnetostrictive/magnetoelastic resonator 76
4.3 Characterization of resonance behavior of magnetostrictive/magnetoelastic resonator 79
4.3.1 Indirect approach for the frequency-domain technique 79

4.3.2 Time-domain technique 106
4.4 Conclusions 114
References 115
5 Synthesis of amorphous magnetostrictive thin film/nanowires using electrochemical deposition method 116
5.1 Introduction 116
5.2 Materials preparation 117
5.3 Electrochemical deposition of amorphous Co-Fe-B thin films 117
5.4 Electrochemical deposition of Co-Fe-B nanobars/nanotubes 122
5.5 Results and discussion 124
5.6 Conclusions 133
References 134
6 Future perspectives and recommendations 136

List of Figures

Figure 1-1 Schematic of different colony counting techniques where the white dots represent the bacteria colonies and the grey circles represent the agar plate 6

Figure 1-2 Illustration of enzyme labeled antibody ELISA 6

Figure 1-3 An illustration of the polymerase chain reaction (PCR) 8

Figure 1-4 Schematic illustration of a typical biosensor system 9

Figure 1-5 A typical prism-based surface plasmon resonance biosensor configuration 11

Figure 1-6 Scheme of frequency vs. signal amplitude of an AW sensor, where f_0 and f_{mass} are the resonance frequency of the sensor without mass load and with mass load, respectively 14

Figure 1-7 Schematic definition of Q value. The resonance peak is at frequency f_0 with a height of h 15

Figure 1-8 Schematic illustration of an acoustic plate mode (APM) device 16

Figure 1-9 Diagram of Lamb wave modes 18

Figure 1-10 Illustration of cantilever array readout by optical beam deflection 21

Figure 1-11 Illustration of a fluid filled micro-cantilever 22

Figure 1-12 Configuration of a magnetostrictive micro-cantilever 22

Figure 1-13 Schematic of working principle of a magnetostrictive biosensor 24

Figure 1-14 (a) Smooth surface; (b) rough surface with trapped liquid particles; (c) equivalent attached liquid layer on the smooth surface. The solid circles represent liquid particles. R denotes the variation of the mountains and valleys where the mountains and valleys were assumed to be evenly and uniformly distributed on the MSP surface. R_{ave} denotes the average surface roughness (i.e. average thickness of the trapped liquid layer) 26

Figure 1-15 Magnetostriction response of a magnetostrictive material: mechanical strain (λ) in relation to external magnetic field (H) 27

Figure 1-16 Schematic structure of a filamentous phage 29

Figure 1-17 Configuration of a typical antibody structure 30

Figure 2-1 Configuration of a network analyzer with an S-parameter test set 38

Figure 2-2 A typical magnitude and phase curve of S_{11} parameter changing with the frequency of an MSP 38

Figure 2-3 Resonance frequency (f_1) of the 1st harmonic mode (n = 1) of MSPs 41

Figure 2-4 $2Lf_1$ in relation to L for the MSPs with different L/W ratios 42

Figure 2-5 The Q value of MSPs with different sizes and geometries 42
Figure 2-6 The length dependence of the resonance frequency ($f_{1,l}$) of first harmonic mode for MSPs in different liquids 43
Figure 2-7 The "$2 \cdot L \cdot f_{1,l}$" in relation to the L for the MSPs with different L/W ratios, where the $f_{1,l}$ is the resonance frequency of the first harmonic mode of MSPs in liquids 44
Figure 2-8 The "$2 \cdot L \cdot f_{1,l}$" in relation to the L/W ratio for the MSPs with different lengths, where the $f_{1,l}$ is the resonance frequency of the first harmonic mode of MSPs in liquids 45
Figure 2-9 $\Delta f_n/\rho_l$ vs. $\sqrt{\eta/\rho_l}$ for two similar MSPs in different liquids 47
Figure 2-10 $\Delta f_n/\rho_l$ vs. $\sqrt{\eta/\rho_l}$ for two similar MSPs in different liquids 48
Figure 2-11 $\Delta f_n/\rho_l$ vs. $\sqrt{\eta/\rho_l}$ for MSPs with the same width but different lengths in different liquids, where the MSPs were operated at first harmonic mode 49
Figure 2-12 Δf_n in relation to $(f_n)^{0.5}$ for an MSP in different media. The size of the MSP is 15.52 mm × 3.78 mm × 30 μm and three harmonic modes (1^{st}, 3^{rd}, 5^{th}) are presented 50
Figure 2-13 The $1/Q$ vs. $\sqrt{\rho_l \eta}$ for two similar sizes of MSPs (MSP-1: 15.52 mm × 3.78 mm × 30 μm and MSP-2: 15.58 mm × 3.76 mm × 30 μm) in different liquids 52
Figure 2-14 $\Delta f_n/\rho_l$ vs. $\sqrt{\eta/\rho_l}$ for MSPs with the same width but different lengths in different liquids, where the MSPs were operated at first harmonic mode 53
Figure 3-1 Schematic illustration of modification of antibodies (top) and the immobilization of the modified antibody onto gold coated MSP (bottom) 58
Figure 3-2 Schematic configuration of the experimental setup for the characterization of the response of MSP biosensor in liquid analyte 60
Figure 3-3 Scheme of (a) the sequences of the analytes through the test chamber (tube); (b) the typical sensor response 61
Figure 3-4 (a) Stable/saturated shift in the resonance frequency shift of an MSP sensor in relation to the population of the analyte. (b) A typical Hill plot obtained from the data shown in Figure (a) 63
Figure 3-5 A typical dynamic dose response of a phage E2 immobilized magnetostrictive biosensor in the size of 1.0 mm × 0.3 mm × 15 μm to increasing population of *S. typhimurium* 66
Figure 3-6 Resonance frequency shifts (Hz) change with the increasing population of the *S. typhimurium* 66
Figure 3-7 Hill plot from the dose response curve 67
Figure 3-8 The dynamic dose response of an antibody immobilized sensor to the increasing population of *E. coli* 67

Figure 3-9 Resonance frequency shifts (Hz) change with the increasing population of the *E. coli* suspensions (cfu/ml) 68
Figure 3-10 Hill plot from the dose response curve 68
Figure 3-11 The dynamic dose response of an antibody immobilized sensor to the increasing population of *S. aureus* 69
Figure 3-12 Resonance frequency shift (Hz) of the sensors with different treatment 70
Figure 3-13 Hill plot from the dose response curve 70
Figure 3-14 A dynamic dose response of an antibody immobilized magnetostrictive sensor to increase populations 71
Figure 3-15 Resonance frequency shift (Hz) of the sensors with different treatment: the antibody immobilized sensor (square) and a reference sensor (dot) change with the increasing population of the *L. monocytogene* suspensions 72
Figure 3-16 The Resonance frequency shift (Hz) of the sensors with different treatment: magnetostrictive biosensors (square), reference sensors (dot), casein blocked controlled sensors (triangle), and BSA blocked controlled sensors (reciprocal triangle) 72
Figure 3-17 Hill plot from the dose response curve showing the kinetics of antibody and bacteria binding 73
Figure 3-18 SEM images of *L. monocetogenes* on (a) the casein controlled sensor; (b) the BSA controlled sensor; (c) the reference sensor (devoid of antibody immobilization), and (d) the antibody-immobilized magnetostrictive sensor 73
Figure 4-1 The equivalent circuit of the device under test (DUT). (a) The overall equivalent circuit. (b), (c), and (d) show the details of the equivalent circuit for three main parts of the circuit shown in (a), where R, L and C are resistor, inductor, and capacitor, respectively 76
Figure 4-2 Frequency dependence of the impedance $Z(\omega)$ of a magnetic resonator in a coil 78
Figure 4-3 Schematic of time domain technique, (a) a pulse current is applied on to a DUT; (b) a voltage across the two ends of the DUT is generated. The voltage changes with the time 78
Figure 4-4 The schematic circuit for (a) the DUT; (b) the reference 80
Figure 4-5 Fitting for the resonance phase behavior of a sensor in the size of 1.0 mm × 0.3 mm × 30 μm in air. The dash lines are the fitting results while the solid lines are the experimental results 82
Figure 4-6 (Left) block diagram of the interrogation device, (right) picture of the interrogation device 83
Figure 4-7 The picture of the circuit built based on the design shown in Figure 4-5 83

Figure 4-8 The holder built on a circuit board, where both reference and DUT channels are included. The backside of the board is grounded 84
Figure 4-9 The graphical user interface (GUI) 85
Figure 4-10 Resonance spectrum of the sensor using different device: (a) phase in relation to frequency; (b) amplitude and gain in relation to frequency where the solid line represents the measured result using network analyzer and the dash line represents the measured result using the indirect approach 86
Figure 4-11 (a) Phase of $Z(\omega)$ frequency in air in relation to frequency in water; (b) gain of $Z(\omega)$ in relation to frequency in air and in water 87
Figure 4-12 Phase signal of MSP in coil in relation to frequency. (a) MSP in size of 0.75 mm × 0.15 mm × 30 μm; (b) MSP in size of 0.5 mm × 0.1 mm × 30 μm. The dash lines are the results for MSPs in water, while the solid lines are the results for MSPs in air 88
Figure 4-13 Schematic configuration of a capacitor in parallel with the DUT 89
Figure 4-14(a) The phase in relation to frequency for an MSP in a coil. The different curves are the results of different capacitors in parallel with the DUT. The capacitance (C_x) of each capacitor is given in this figure 89
Figure 4-14(b) The gain in relation to frequency for an MSP in a coil. The different curves are the results of different capacitors in parallel with the DUT. The capacitance (C_x) of each capacitor is given in this figure 90
Figure 4-15 (a) Phase in relation to frequency; (b) absolute value of phase in relation to frequency. In (a) from top to bottom, the curves correspond the increase in the capacitance of C_x 92
Figure 4-16 The phase peak amplitude in relation to capacitance of C_x 92
Figure 4-17 Schematic configuration of a capacitor in series with the DUT 93
Figure 4-18(a) The phase in relation to frequency for an MSP in a coil. The different curves are the results with different capacitors in series with the DUT. The capacitance of each capacitor is given in this figure 93
Figure 4-18(b) The gain in relation to frequency for an MSP in a coil. The different curves are the results with different capacitors in series with the DUT. The capacitance of each capacitor is given in this figure 94
Figure 4-19 The simulation of phase in relation to frequency. The curves from top to bottom correspond to the increase in the capacitance of C_x 94
Figure 4-20 Phase peak amplitude in relation to capacitance of C_x 95
Figure 4-21 Schematic configuration of a resistor in parallel with the DUT 95

Figure 4-22(a) The phase in relation to frequency for an MSP in a coil. The different curves are the results of different resistors in parallel with the DUT. The resistance of each resistor is given in this figure 96
Figure 4-22(b) The gain in relation to frequency for an MSP in a coil. The different curves are the results of different resistors in parallel with the DUT. The resistance of each resistor is given in this figure 96
Figure 4-23 The simulation of phase in relation to frequency. The curve moves from bottom to top corresponding to the increase in the resistance of R_x 97
Figure 4-24 Phase peak amplitude in relation to resistances of R_x 98
Figure 4-25 Schematic configuration of a resistor in series with the DUT 98
Figure 4-26(a) The phase in relation to frequency for an MSP in a coil. The different curves are the result of different resistors in series with the DUT. The resistance of each resistor is given in this figure 99
Figure 4-26(b) The gain in relation to frequency for an MSP in a coil. The different curves are the result of different resistors in series with the DUT. The resistance of each resistor is given in this figure 99
Figure 4-27 The phase in relation to frequency for an MSP in a coil. The curves from the top to the bottom correspond to the increase in the resistance of R_x 100
Figure 4-28 Phase peak amplitude in relation to resistances of R_x 100
Figure 4-29 New design for DC and AC coils 101
Figure 4-30 Phase in relation to frequency under different DC current 102
Figure 4-31 (a) Resonance frequency in relation to DC for the same sensor; (b) phase peak amplitude in relation to DC for the same sensor. 102
Figure 4-32 Schematic configuration I of the holder where two sensors (MSP-1 and MSP-2) were put in one coil 103
Figure 4-33 The phase signal vs. frequency for two sensors (MSP-1 and MSP-2) in one coil .. 103
Figure 4-34 Schematic configuration II of the holder where two coils are connected in parallel 104
Figure 4-35 The phase signal vs. frequency for two coils: coil-1 and coil-2 connected in parallel. The MSP-1 was placed in coil-1 and MSP-2 was placed in coil-2 104
Figure 4-36 Schematic configuration III of the holder where two coils were connected in series 105
Figure 4-37 The phase signal vs. frequency for two coils: coil-1 and coil-2 connected in series. The MSP-1 was placed in coil-1 and MSP-2 was placed in coil-2 105
Figure 4-38 Resonance frequency shift (Hz) change with the increasing population of the *S. typhimurium* suspensions 106
Figure 4-39 Schematic definition of a square pulse as a function of time 107

Figure 4-40 Schematic diagram of an FT magnitude spectrum of a square pulse 107
Figure 4-41 (a) Signal amplitude vs. time; (b) signal amplitude vs. frequency 108
Figure 4-42 Schematic block diagrams for the time-domain interrogation device 108
Figure 4-43 (a) Picture of the circuitry based on the design; (b) picture of circuitry in the metal box as shown in Figure 4-44(a) 109
Figure 4-44 (a) Picture of the holder; (b) schematic diagram of the driving and pick-up coils 109
Figure 4-45 The graphical user interface (GUI) 110
Figure 4-46 The power spectrum vs. frequency for an MSP sensor 111
Figure 4-47 The power spectrum vs. frequency for (a) two sensors (MSP-1 and MSP-2) in air and in water; (b) two sensors (MSP-3 and MSP-4) in air and in water 112
Figure 4-48 The power spectrum vs. frequency under different pulse voltages for an MSP sensor 113
Figure 4-49 The dose response of a magnetostrictive phage immobilized sensor (square), reference sensor (dot), and casein blocked sensor (triangle) 114
Figure 5-1 Electrochemical cell for Co-Fe-B thin film deposition 118
Figure 5-2 XRD patterns of Co-Fe-B thin films with different deposition currents 120
Figure 5-3 XRD patterns of Co-Fe-B thin films with different amount of DMAB 121
Figure 5-4 XRD patterns of Co-Fe-B thin films with different amount of $FeSO_4$ 122
Figure 5-5 Template synthesis of Co-Fe-B nanobars/nanotubes 123
Figure 5-6(a) Partially gold covered template, deposition current: 15 mA, deposition time: 1 min, initial concentration 125
Figure5-6(b) Partially gold covered template, deposition current: 15 mA, deposition time: 3 min, initial concentration 125
Figure5-6(c) Partially gold covered template, deposition current: 15 mA, deposition time: 6 min, initial concentration 126
Figure 5-6(d) Partially gold covered template, deposition current: 15 mA, deposition time: 15 min, initial concentration 126
Figure 5-6(e) Partially gold covered template, deposition current: 1 mA, deposition time: 3 min, initial concentration 127
Figure 5-6(f) Partially gold covered template, deposition current: 5 mA, deposition time: 3 min, initial concentration 127
Figure 5-6(g) Partially gold covered template, deposition current: 10 mA, deposition time: 15 min, initial concentration 128
Figure 5-6(h) Partially gold covered template, deposition current: 15 mA, deposition time: 6 min, 1/4 initial concentrations 128